Nuclear Engineering and Design 429 (2024) 113676

Contents lists available at ScienceDirect

Nuclear Engineering and Design

journal homepage: www.elsevier.com/locate/nucengdes

Analysis of the experimental tests performed at NACIE-UP facility through a novel CFX-RELAP5 codes coupling

T. Del Moro [a,*], P. Cioli Puviani [b], B. Gonfiotti [c], I. Di Piazza [c], D. Martelli [c], C. Ciurluini [a], F. Giannetti [a], R. Zanino [b], M. Tarantino [c]

[a] Department of Astronautical, Electrical and Energy Engineering DIAEE, Sapienza University of Rome, Corso Vittorio Emanuele II, 244, 00186 Rome, Italy
[b] NEMO Group, Dipartimento Energia, Politecnico di Torino, Corso Duca degli Abruzzi, 24, 10129, Torino, Italy
[c] ENEA Brasimone, 40032 Camugnano, Bologna, Italy

ARTICLE INFO

Keywords:
CFD
STH
HLM
Natural circulation
Gas Lift
Codes coupling

ABSTRACT

The design and safety assessment of Lead-cooled Fast Reactors (LFRs), being one of the Generation IV technologies, must be supported by extensive experimental campaigns. Such activities are necessary to completely understand the physical phenomena involved in such reactors, as well as to properly develop new numerical tools or validate the pre-existent ones. From the experimental point of view, ENEA Research Center of Brasimone is one of the most active institutions, thanks to its experimental platforms and know-how maturated since the early 2000s. From the numerical point of view, Computational Fluid Dynamics (CFD) codes are the most suitable ones to analyze some phenomena expected in a Heavy Liquid Metal (HLM)-cooled reactor, such as the complex 3D phenomena occurring within the pools or the core fuel assemblies. In addition, the fluid thermal conduction, usually neglected in a System Thermal-Hydraulic (STH) code, can assume a significant importance in some transient scenarios, e.g., loss of flow accidents with transition from forced to natural circulation. However, the safety analysis of the LFRs should still rely on the use of STH codes because of their lower computational cost compared to the CFD codes, also considering the high number of transient evolutions to be analyzed for the purpose of the reactor licensing. At ENEA Brasimone, a novel coupling approach has been developed to couple the CFD code Ansys CFX with the STH code RELAP5/Mod3.3. The coupled tool aims at exploiting the advantages of the two families of codes. It adopts a multi-scale approach to simulate in detail some circuit components while performing system-level analysis, so as to keep an acceptable computational time. The coupling technique is based on ad-hoc user routines written in FORTRAN and implemented in Ansys CFX, which acts as the master code. The user routines take care of time step management, data exchange, RELAP5 execution, and error checking. The goal of this paper is to assess the simulation capabilities of the coupled tool by reproducing a forced-to-natural-circulation transition test, carried out at the NACIE-UP facility, with LBE as working fluid. The work has been realized in the framework of the IAEA Coordinate Research Project-I31038, named "Benchmark of Transition from Forced to Natural Circulation Experiment with Heavy Liquid Metal Loop".

1. Introduction

The increasing demand of energy requires sustainable, safe, and reliable energy sources, necessitating the advancement of innovative technologies. Within the nuclear field, the Generation IV (Generation IV International Forum) reactors are possible solutions to fulfil the requirements of waste reduction, sustainability, reduction of proliferation risk, and the adoption of passive safety systems. Lead-cooled Fast Reactors (LFRs) (Lorusso et al., 2018) stand as one of the most economically competitive solutions, relying mostly on their compactness and intrinsic safe operation, thanks to the large adoption of passive safety systems.

Several LFR concepts are currently under development worldwide, and their construction is foreseen to be completed by the end of '30 s. Relevant examples are:

- the 300 MW_{th} Advanced Lead-cooled Fast Reactor European Demonstrator (ALFRED) (Alemberti et al., 2015; Frignani et al.,

* Corresponding author.
E-mail address: tommaso.delmoro@uniroma1.it (T. Del Moro).

https://doi.org/10.1016/j.nucengdes.2024.113676
Received 19 June 2024; Received in revised form 25 October 2024; Accepted 25 October 2024
Available online 30 October 2024

2017; Frignani et al., 2019), designed by the FALCON (Fostering ALFred CONstruction) Consortium, of which ENEA is a partner, together with ANSALDO Nucleare and RATEN ICN;
- the Westinghouse LFR, designed by Westinghouse Electric Company (WEC) (Westinghouse);
- the *new*cleo mini LFR (30 MWe) and small LFR (200 MWe) (https://www.newcleo.com/);
- BREST-OD-300 (Dragunov et al., 2012), which is under construction in Russia.

Experimental campaigns have been conducted, and many others are planned to be performed, aiming at understanding the main phenomena governing the pool-type reactors, as well as the heat transfer characteristics for each core and steam generator design. ENEA Brasimone Research Center (R.C.) is one of the most active research institutes on this topic thanks to the wide availability of experimental facilities and know-how developed since the early 2000s. Examples of experimental facilities are NACIE-UP (Di Piazza et al., 2019) and CIRCE (Lorusso et al., 2021), which are LBE-cooled separate and integral effects test facilities, respectively.

Computational tools are required to support the design and safety assessment of the reactors. CFD codes are currently adopted to support the Thermal-Hydraulic (TH) analyses of components in nuclear reactors, as well as to better understand the behavior of the fluids in a 3D geometry, such as the pool-type configuration of the LFRs. However, no CFD code is currently validated for the safety analysis of nuclear reactors, in contrast to System Thermal-Hydraulic (STH) codes, such as RELAP5 (Information System Laboratories, 2003) and CATHARE (CEA, 2019), that have been extensively used for Light Water Reactors (LWRs) licensing. The main advantage of CFD codes is the possibility to analyze in detail the TH behavior of components and systems thanks to the resolution of 3D equations for mass, momentum, and energy, but at the cost of high computational time. Instead, STH codes do not allow to fully reproduce a system where 3D effects are important. As a matter of fact, the fundamental assumption behind STH codes is that the main TH quantities, e.g., pressure, velocity, etc., within a "cell" of few centimeters in size can be averaged in a single value representative of the whole cell. Therefore, a 1D formulation of the conservation equations is solved, and on a number of cells that is typically much lower than a CFD domain, leading to a relatively low computational cost. Moreover, another typical assumption of the STH codes consists in neglecting the conduction inside the fluid, thus not allowing to properly model low-Peclet number flows, i.e., loss of flow transients, where the thermal conduction can be relevant compared to the convection.

Several CFD-STH coupled approaches have been already implemented with different codes (Pucciarelli, 2020), adopting various STH codes, such as RELAP5, ATHLET (GRS, 2021), TRACE (USNRC, 2008), SAM (Argonne National Laboratory, xxxx) and CFD codes, such as Ansys Fluent (ANSYS FLUENT, 2009), Ansys CFX (ANSYS CFX-Solver Theory Guide, 2011), STAR-CCM+ (Siemens, 2021). Their field of application was mainly GEN-III and GEN-IV technologies. Aumiller et al. (Aumiller et al., 2001) pioneered the coupling of RELAP5-3D© with CFX, introducing a methodology and presenting a proof-of-principle calculation that demonstrated the feasibility of this approach for nuclear reactor analysis. Since then, several research activities have been focused on the overcoming of the inherent challenges related to the code coupling, such as data transfer, temporal synchronization, and interface stability. Bertolotto et al. (Bertolotto et al., 2009) advanced this field by investigating single-phase mixing using a directly coupled CFX-TRACE, which enabled more detailed predictions of flow behavior in complex geometries, further supporting its application to transient scenarios. An alternative approach was provided by Forgione et al. (Forgione et al., 2019), who developed a MATLAB© interface coupling RELAP5 and FLUENT codes and applied it to the CIRCE-HERO facility, confirming the method's effectiveness in simulating complex thermal–hydraulic phenomena in Heavy Liquid Metal (HLM) reactors, such as natural circulation and thermal stratification. A further example of RELAP5/FLUENT coupling is reported in (Toti et al., 2016), where a preliminary validation of the method was carried out against experimental data from TALL-3D facility (Grishchenko et al., 2015). Another notable advancement is the one proposed by Li et al. (Li et al., 2014), who also conducted a preliminary study on coupling FLUENT with RELAP5 through Dynamic Link Library (DLL) technology and Fluent User Defined Function (UDF). They set up an explicit coupling method and validated it by test cases such as a pipe blowdown scenario, showing accuracy for both single and two-phase flow problems. More recent developments by Grunloh and Manera (Grunloh and Manera, 2016; Grunloh and Manera, 2017) introduced a multi-scale domain overlapping strategy, which allows seamless integration of CFD (STAR-CCM +) and system codes (TRACE) by dynamically adjusting the spatial resolution at the interface, providing enhanced stability and accuracy for transient simulations relevant to nuclear safety. Recent studies by Huxford et al. (2023) (Huxford et al., 2023) and (2024) (Huxford et al., 2024) further validated these hybrid domain overlapping approaches, coupling CFD and STH codes (i.e., SAM) with the aim of performing reactor transient analysis. They achieved reliable predictions in various safety-relevant accidental scenarios.

At the ENEA Brasimone R.C., a novel coupling approach between the CFD code Ansys CFX and the STH code RELAP5/Mod3.3 has been developed, with the aim to realize a lean tool capable of performing system-level analyses and focusing at the same time on a particular component or fluid portion that requires a CFD level modeling. The tool adopts in-house developed scripts for the data post processing and exchange, completely managed by the Ansys CFX code which is the master code. Compared to the previously developed coupling methods, these in-house scripts offer greater flexibility and customization, and the possibility to optimize the data exchange. Its final goal is to reproduce the TH behavior of HLM-cooled reactors by exploiting the advantages of the two families of codes and adopting a multiscale approach (Moreau et al., 2019).

The work presented in this paper serves as a step towards the validation of the coupling architecture developed by ENEA, by using the experimental data produced by the NACIE-UP facility, located at the ENEA Brasimone R. C. University of Pisa developed and applied a RELAP5-Ansys Fluent coupling tool to simulate the NACIE-UP facility (Martelli et al., 2017). However, they simulated different experiments than the ones presented in this paper, and the data exchange relies on an external platform (MATLAB©)The numerical application presented in this paper consists in the post-test analysis of the experimental data released in the framework of the IAEA international Coordinate Research Project I31038, named "Benchmark on Transition from Forced to Natural Circulation Experiment with Heavy Liquid Metal Loop". The application of the coupled tool intends to increase maturity and confidence in adopting CFD-STH coupling, to support the design, transient analysis, and safety assessment of LFRs.

2. NACIE-UP facility

2.1. NACIE-UP facility description

NACIE-UP (Di Piazza et al., 2022) is a Lead-Bismuth Eutectic (LBE) cooled rectangular loop with an overall height of 7.7 m. It is composed of an electrical Fuel Pin Bundle Simulator (FPBS) located at the bottom of the riser section, an expansion vessel at the top, and a double wall tubes Heat Exchanger (HX) installed at the top of the downcomer pipeline. LBE is moved by the gas lift, consisting in the injection of argon in the riser to enhance the natural circulation. The facility is equipped with several Thermo-Couples (TCs) monitoring the temperatures of the loop and within the FPBS. A schematic drawing of the facility is shown in Fig. 1, where the qualitative location of the main loop TCs is indicated, as well as of the Pressure Transducers (PTs) at the riser top and bottom. The mass flow rate is measured by a prototypical Thermal mass Flow

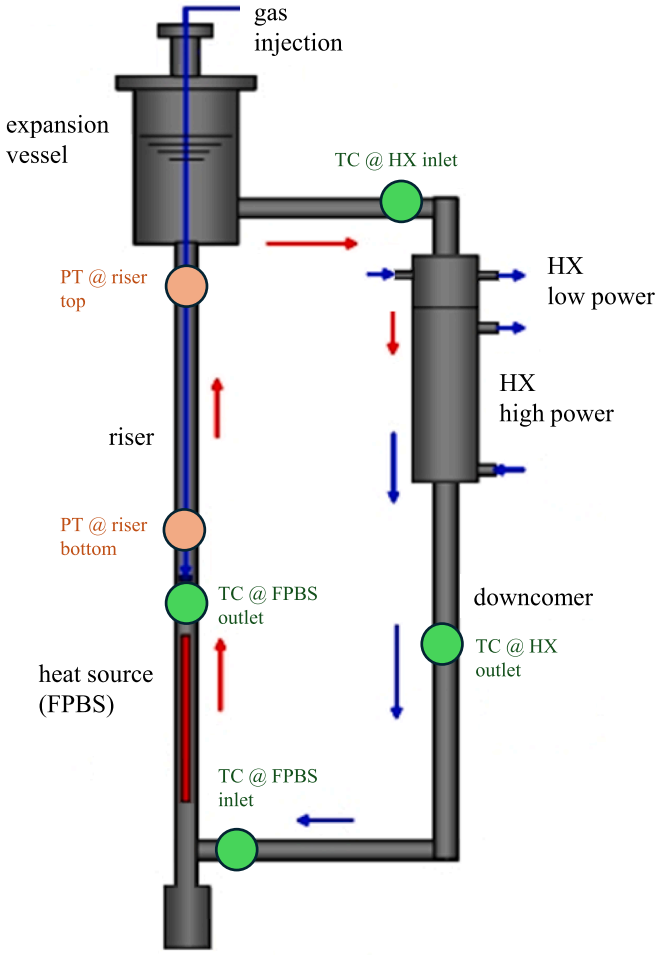

Fig. 1. Schematic drawing of the NACIE-UP primary loop (Di Piazza, 2019).

Meter (TFM) (Cioli Puviani et al., 2024) developed by ENEA in collaboration with Thermocoax. It is based on the energy balance between the power delivered by the instrument to the fluid and the temperature variation across the component.

The FPBS is composed of 19 wire-spaced electrical rods, arranged in a triangular lattice with a pitch-to diameter ratio of about 1.28. The pin diameter is equal to 6.55 mm, while the wire diameter is 1.75 mm, and it is helicoidally twisted around the pin with a helical pitch of 262 mm. Each pin is 2000 mm long with an active length of 600 mm. In the "pre-active" length about ~8–10 % of the overall power is provided to the fluid because of the combined effect of axial conduction along the pin and the joule effect, having this region a lower electric resistance than the active one but still non null. The pins are kept in position by a grid downstream the FPBS. The bundle is contained in a hexagonal wrapper. TCs in the FPBS are located on Plane 1, Plane 2 and Plane 3, respectively at 38, 300 and 532 mm from the beginning of the active length. A selected pin, i.e., Pin 3, is equipped with more wall-embedded TCs, one every 43.7 mm after the Plane 1 (Di Piazza et al., 2022). The drawing is reported in Fig. 2, where the active and the non-active regions are highlighted, along with the instrumented planes in the active region.

The expansion vessel must accommodate the thermal expansions of the LBE and keep the system pressure thanks to a volume of cover gas. It is equipped with two level sensors that fix the LBE level during the filling of the facility.

The HX is a shell and tube type, composed of 7 double wall tubes, with a gap between the LBE and the water (secondary coolant) that is filled with AISI 316L powder and pressurized air. LBE flows tube side from the top to the bottom of the component. There are two parts composing the shell side: a "low power section" (0–30 kW), where the secondary fluid moves in cross flow with respect to the LBE, and a "high power section" (30–250 kW), where the water flows shell side in countercurrent with respect to the LBE. The secondary side is a closed loop working with pressurized water at 16 bar, equipped with a circulation pump, a pressurizer, and an air cooler. In these experiments, only the "high power section" of the HX has been used.

2.2. Description of the experimental tests

All the experimental tests (named ADP06 and ADP10) (Marinari et al., 2019) (Angelucci et al., 2018) analyze the transition from an initial steady state in forced circulation – where the fluid flow is enhanced by the gas injection in the riser line – to a second steady state during which natural circulation is established. The transition starts when the gas injection is stopped. This causes a sudden reduction of the LBE mass flow rate, since the only lasting driving force to promote the LBE flow is natural circulation. Since the FPBS power (uniformly distributed among the 19 pins) remains constant during the test, the LBE temperature downstream of the FPBS increases, and in the long term the riser temperature increases as well. At the same time, the mass flow reduction produces a temperature decrease in the cold leg section.

For all the tests, in the initial steady state, the gas is injected at a constant flow rate of 10 Nl/min. Water in the secondary side is kept at 16 bar, with a constant temperature at the HX inlet of 170 °C, and the volumetric flow rate is 10 m^3/h. At t = 0 s, the gas flow rate drops to zero in 1 s, while all the other parameters remain constant. After the transition, a new steady state condition is achieved, and it is kept for more than 30 min. A summary of the experimental conditions is reported in Table 1, where "Steady state 1" and "Steady state 2" refer to the steady state conditions at the beginning and end of the transient, respectively.

The experimental tests differ from each other in the number and location of the active pins (shown in Fig. 3):

- in the ADP10 test all the 19 pins are switched on (the fuel assembly is symmetrically heated). The total power is 30 kW and the average heat flux on the pins' surface is 127.9 kW/m^2.
- in the ADP06 test only the 7 central pins are switched on, but the total power is the same as the previous test. The average heat flux on the pins' surface is 347.1 kW/m^2.

Temperature values are measured in several points of the loop by thermocouples that have an accuracy of ± 1.5 °C. The LBE mass flow rate is measured by a thermal flow meter whose uncertainty depends on the power provided by the heating element, the temperature at the instrument inlet, and the mass flow rate. The uncertainty can be evaluated by a formula presented in Ref. (Cioli Puviani et al., 2024), that results in a maximum value of about 5 % for the considered experiments.

3. Ansys CFX-RELAP5 coupled tool

The coupling between Ansys CFX and RELAP5 (Cioli Puviani et al., xxxx) has been realized through in-house developed FORTRAN routines that are called in specific "time-locations" of the Ansys CFX run (which is the master of the coupling process), and in turn they call specific executables written in Python to run and post-process RELAP5 results. The routines must guarantee the synchronization between the codes during the coupled simulation execution and data exchange. The coupling strategy is based on a two-way connection, with partitioned and sequential solutions. The spatial domain approach is non-overlapping (or decomposition), while the time advancing scheme adopted in this analysis is semi-implicit. Other details are reported in Table 2, where the classification follows the guidelines of Ref. (Di Piazza et al., 2019), and a schematic representation of the semi-implicit coupling procedure is depicted in Fig. 4, where the following acronyms are used:

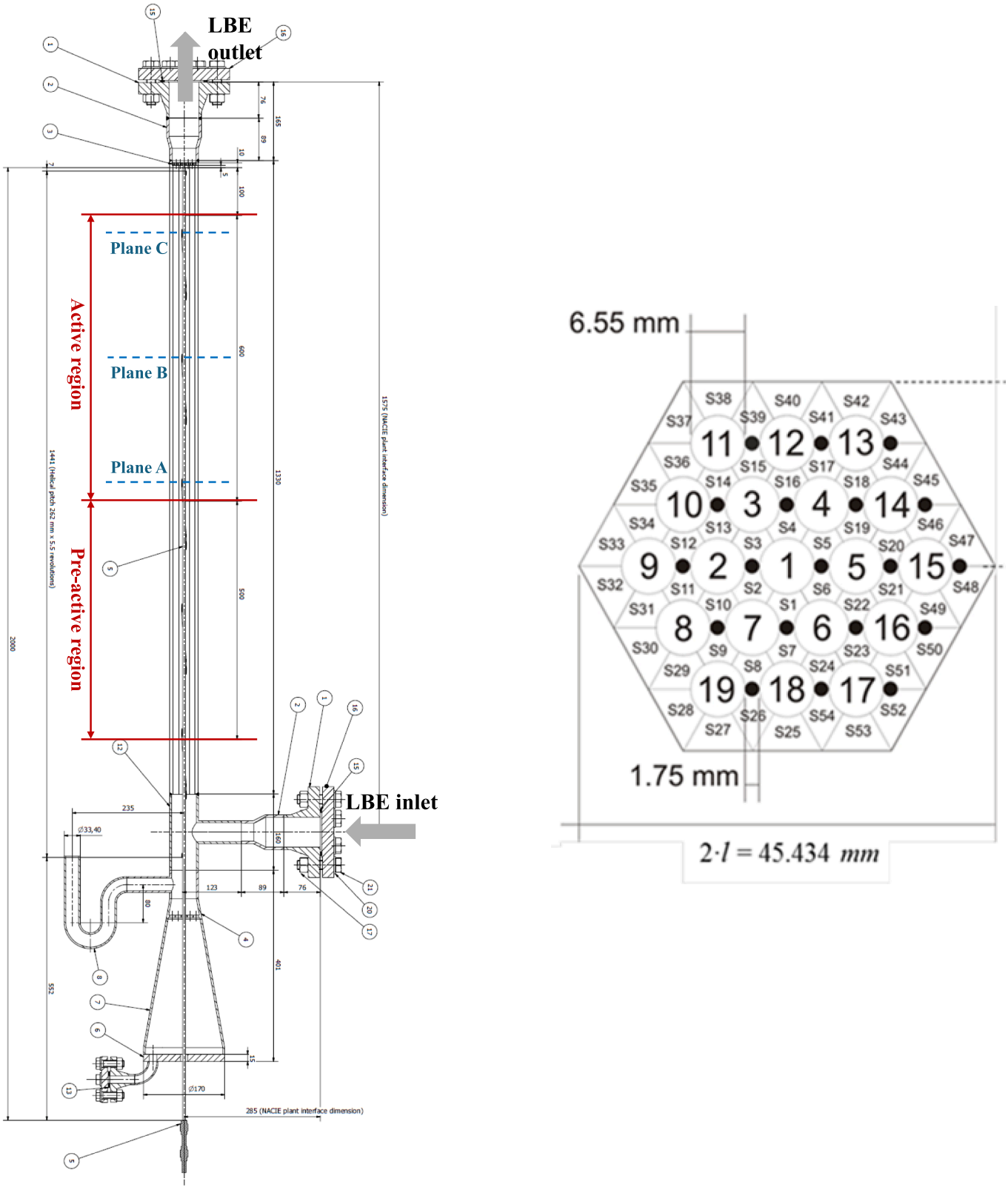

Fig. 2. NACIE-UP FPBS layout (left) and cross section view (right).

- JBR: Junction Box Routine. It is a generic FORTRAN script. In the coupled simulation, several JBRs are called in specific time locations of the CFX run, each one performing different tasks.
- SOTT: Start Of The Timestep. It is a CFX time location (see CFX manual (ANSYS CFX-Solver Theory Guide, 2011) for the definition of "time location") just before the code starts to solve the equations at each time step. It applies only in transient runs, and it is related to the "outer loop";

Table 1
Experimental boundary conditions for ADP10 and ADP06 tests.

Parameter	ADP10		ADP06	
	Steady state 1	Steady state 2	Steady state 1	Steady state 2
$\dot{m}_{gas}$ [Nl/min]	10	0	10	0
$\dot{Q}_{tot}$ [kW]	30	30	30	30
q'' [kW/m^2]	127.9	127.9	347.1	347.1
$\dot{m}_{H_2O}$ [m^3/h]	10	10	10	10
T_{inlet,H_2O} [°C]	170	170	170	170
p_{H_2O} [bar]	16	16	16	16

- SOCL: Start Of Coefficient Loop. It is a CFX time location at the beginning of the internal cycles of the solver. For transient runs, it is related to the "inner loop".

Further information on the coupling tool can be found in Ref. (Cioli Puviani et al., xxxx).

A semi-implicit scheme consists in iterating the same timestep (*j*) until the difference between the boundary conditions (BCs) passed to RELAP5 in two consecutive iterations (*i* and *i-1*) is lower than a tolerance (*tol*, see equation (1)) chosen by the user, or a user defined maximum number of internal cycles is reached.

$$\frac{\left|X_i^j - X_{i-1}^j\right|}{\left|X_i^j\right|} < tol \tag{1}$$

In the equation *X* indicates a generic BC, and it can represent a TH quantity such as mass flow rate, temperature, pressure, heat flux etc. Since these quantities have different magnitudes and *tol* is a unique parameter for all the exchanged BCs, the relative difference and not the absolute one is considered at the end of each iteration to check the convergence of the calculations.

During the internal iterations of the current timestep, the BCs are not constant across the codes. Instead, they account for the results coming from the other code within the same timestep. For example, the RELAP5 timestep may be a fraction of the coupling timestep. For this, its BCs are imposed as a linear interpolation between the results at the end of the previous timestep and those obtained from Ansys CFX at the end of the current internal iteration. More specifically, the CFX results, imposed on RELAP5 as BCs, are averaged at the boundary surfaces. They are not stored in an external data file but directly written in RELAP5 by means of an in-house Phyton written executable.

For Ansys CFX, the coupling time step is adopted. Thus, RELAP5 results, imposed as BCs, must be read and passed only once. They are contained in an external text file, unlike the CFX ones. The 1D BCs coming from RELAP5 are multiplied to a non-dimensional 3D fully developed profile that was preliminary calculated through a stand-alone CFX simulation. The CFD solver, using an implicit method for solving equations, inherently accounts for variations in boundary conditions within a single timestep.

Each new coupled timestep begins with the execution of the STH timestep rather than the slower CFD one, assuming constant BCs as in an explicit approach. This method allows Ansys CFX to receive the semi-implicit boundary condition effects from the very first iteration. Convergence is evaluated based on the BCs in Ansys CFX, provided by RELAP5. As a result, it is possible to meet the tolerance threshold even after the first CFD internal iteration, following the new RELAP5 run. In principle, this allows the coupling methodology to also work with just a single CFD internal iteration, minimizing Ansys CFX computational time.

The semi-implicit scheme allows in principle to adopt larger timesteps compared to the explicit scheme (Pucciarelli, 2020) because it keeps into account the BC values at the end of the timestep, allowing to iterate the same timestep in case strong gradients occur without oscillations in the results. In the semi-implicit scheme, the boundary conditions are passed as time dependent tables, thus allowing RELAP5 to linearly interpolate the boundary conditions when running with a fraction of the coupling timestep, while Ansys CFX adopts an implicit resolution of the equations. The linear interpolation is adopted for the RELAP5 BC because of the availability of only two points (initial and final) and because the relatively small timestep size makes this assumption valid. The semi-implicit time advancing scheme has been selected because of its greater robustness and stability compared to the explicit one, which in turn shows oscillations in the results when calculations are carried out with the same coupling time step. Moreover, the semi-implicit time scheme developed in this work allows to save computational time in case of long simulations, in particular when a steady state is approached, since the coupling run can converge without repeating the same timestep and with a single "outer loop" iteration. The results discussed in the following can be considered as an improvement with respect to the work presented in Ref. (Cioli Puviani et al., xxxx),

Table 2
Coupled methods classification.

Code Integration	Partitioned Solutions
Coupling Execution	In-line approach
Synchronization	Sub-cycling approach
Information Exchange Type	Sequential coupling
Spatial Domains	Non-overlapping domain
Numerical Scheme	Semi-implicit

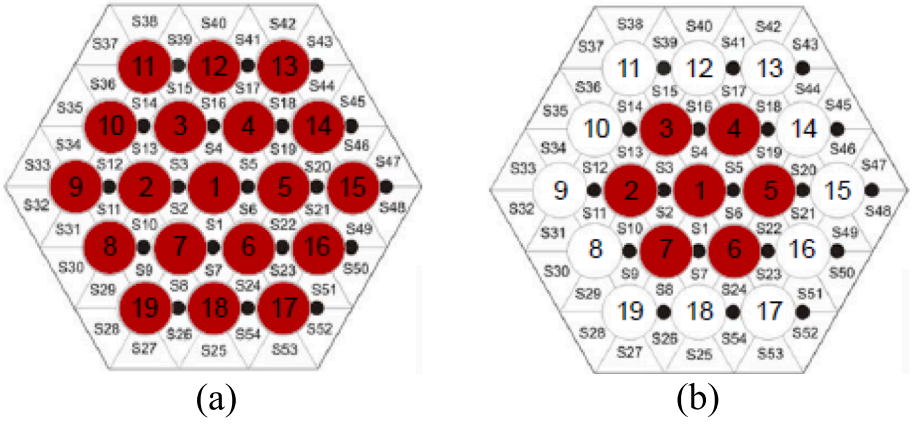

Fig. 3. Active pins (in red) during ADP10 (a) and ADP06 (b) tests (Di Piazza et al., 2022). (For interpretation of the references to colour in this figure legend, the reader is referred to the web version of this article.)

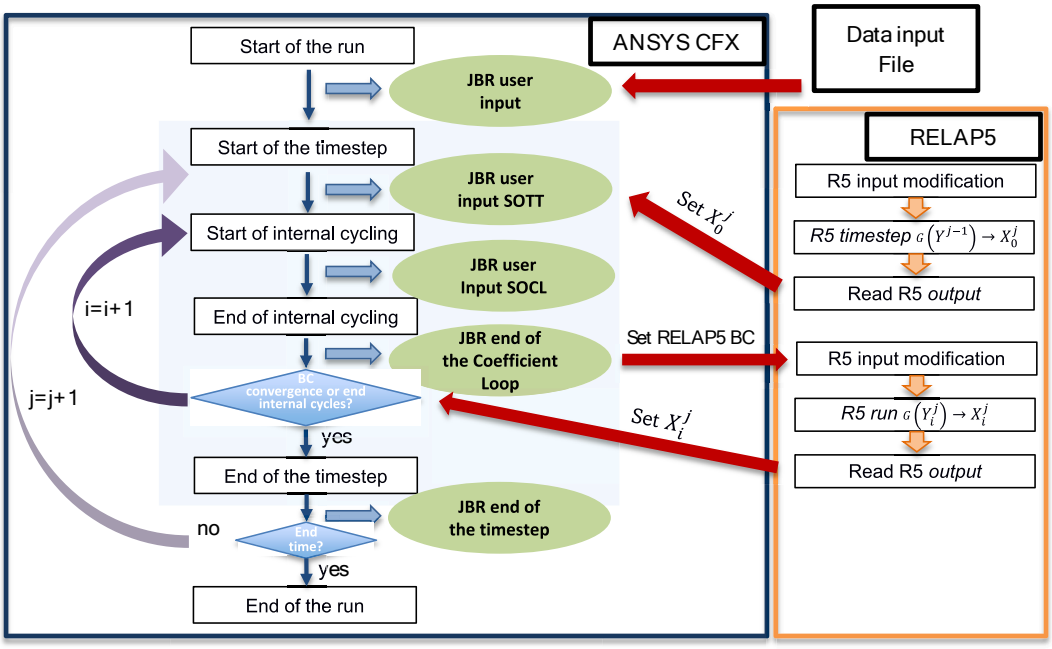

Fig. 4. Coupling procedure in the semi-implicit numerical scheme (Cioli Puviani et al., xxxx).

compared to which both the stand-alone models and the coupling methodology have been refined.

The decomposition domain approach adopts a division of the domain in two independent portions each solved by one of the two codes. Information exchange happens at the boundaries of the two domains. The RELAP5 boundary conditions of pressure and temperature are imposed by two time-dependent volumes, and they are calculated as the surface average on the CFD domain boundaries. The Ansys CFX boundary conditions of mass flow rate and temperature are imposed by applying a non-dimensional map to the 1D values coming from the RELAP5 timestep.

4. Numerical models

4.1. CFD MODEL

The CFD domain is limited to the 600 mm of the active region of the FPBS because of the high computational cost of the simulation. The simulated domain comprehends the LBE (OECD/NEA, 2015) fluid region, the external solid wrapper (AISI316L) that encloses the pin bundle, the wires (AISI316L) and the pins, considering three different materials for the solids (Table 3). The effect of the Inconel600 inside the pin has been neglected and the region included a single Bohrium Nitride (BN) domain (see the schematic of the interior of the pin in Fig. 5).

To limit the number of nodes, the mesh has been decomposed in different bodies in both the axial and radial directions to achieve a structured mesh on each region. The cost of this operation is the high number of interfaces, which also limits the number of partitions in which the coupled simulation can be run to keep under control the time

Table 3
Diameters of the different parts of the pin in the active region (Di Piazza et al., 2022).

Part	*Internal diameter [mm]*	*External diameter [mm]*
Clad (AISI316L)	5.08	6.55
Heating tube (Inconel600)	3.35	3.53
Central conductor (Copper)	–	2.31
1st insulant layer (BN)	2.31	3.35
2nd insulant layer (BN)	3.53	5.08

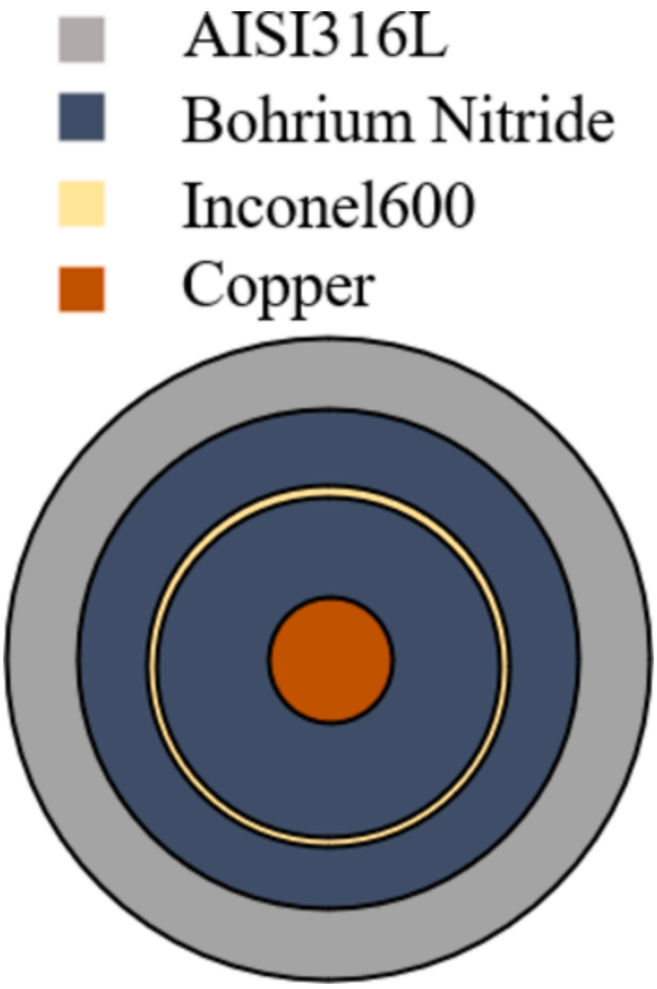

Fig. 5. Schematic of the pin materials.

needed for interface interpolation.

At the FPBS inlet, a fully developed velocity and temperature distribution is imposed. They are obtained by a previously conducted simulation – including two helix pitches upstream of the active region – to retrieve the condition at the FPS inlet. The selected turbulence model is the *SSTk* $-\omega$ (Cioli Puviani et al., 2022) with a constant Pr_t of 1.5. Previous sensitivity analyses showed negligible differences in the range 1.5 – 2 (Martelli et al., 2017). On the external wall of the solid structure, an adiabatic condition is imposed. The fluid boundary layer at the wall is resolved with a $y^+ \sim 1$ on all the fluid–solid boundaries. The defaults option of the CFX solver are adopted leading to a coupled solver that implements the Rhie-Chow algorithm. The Upwind advection scheme implemented in CFX is adopted.

A grid independence study (Table 4) has been carried out, considering the ADP10 initial steady state conditions, to evaluate the number of nodes that represents a compromise between accuracy and computational time consumption. Different meshes have been considered starting from the *Reference* one and varying the near wall treatment and the element size of the mesh in the radial (*Radial ref*) and axial (*Axial ref*) direction. The *Coarse improved* mesh (shown in Fig. 6) composed of 4.5 M nodes has been selected to reduce as much as possible the mesh dimension but achieving a discrepancy lower than 10 % with respect to the most refined meshes.

The CFD stand-alone model is adopted only for the analysis of the steady states while the STH and coupled simulations reproduce the entire transient or a time window of the transient. In the following, the CFD results are presented only for the first steady state of the different tests, since the scope of the paper is to present the coupled tool results.

4.2. RELAP5 model

A model of NACIE-UP facility has been realized through the RELAP5/Mod3.3 code, properly modified to implement HLMs thermo-physical properties and the coexistence in the same hydraulic volume of HLMs and non-condensable gases (Oriolo, 2000; Martelli et al., 2019). The model is constituted by PIPE components that model the fluid region, connected by SINGLE JUNCTION components, while the solid parts are modelled through HEAT STRUCTURES. Heat losses have been considered using as BCs a heat transfer coefficient and a room temperature equal to 8 W/(m^{2}K) and 10 °C, respectively, which are identical for all the simulations. The mesh size is comprised between 5 cm in the active regions (i.e., FPBS and HX, where significant heat exchange and thermal gradients are expected), and a maximum value of 12 cm in the non-active ones (i.e., the rest of the loop where the temperature is almost constant), with a smooth transition between the minimum and the maximum values. The sliced modeling approach (Ciurluini et al., 2024) has been adopted for the entire facility to well capture the behavior of the system under natural circulation conditions. Only the active part secondary side of the HX has been modeled, while the inlet temperature and mass flow rate, and the outlet pressure are imposed by two TIME DEPENDENT VOLUMES and one TIME DEPENDENT JUNCTION. The thermal conductivity of the gap between the coaxial tubes in the HX – filled with stainless steel powder and pressurized air – is evaluated through the following formula (Forgione et al., 2019):

Table 4
Grid independence study of the FPBS CFD model.

	Coarse	Coarse improved	Reference	Radial ref	Axial ref
n° of nodes [M]	4.2	4.5	6.4	33.5	29.3
Δp [mbar]	28.4	31.1	31.4	33.6	33.8
ΔT in-out [°C]	80.1	80.3	80.3	80.3	80.4
T point [°C]	319.0	321.2	322.5	323.1	323.7

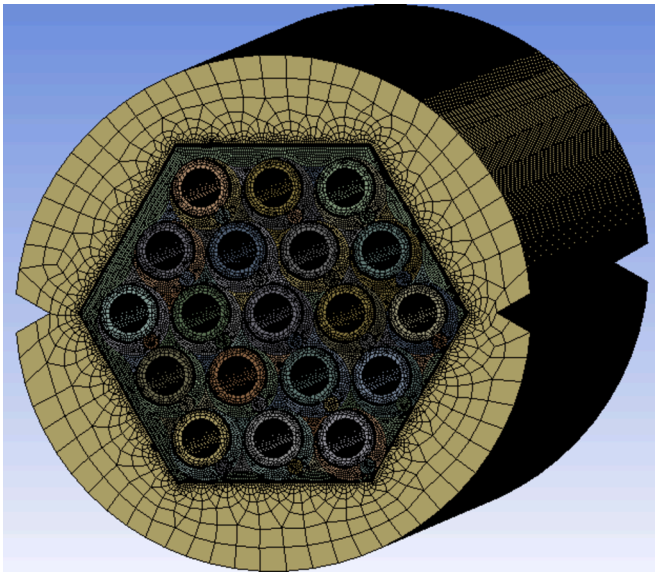

Fig. 6. Coarse improved mesh.

$$k_{powder} = 0.3 + 0.005 \bullet (T - 200) \tag{2}$$

where T is in °C and k is in W/(m·°C). A graphical representation of the nodalization is given in Fig. 7.

Since RELAP5 allows the user to insert Reynolds-dependent friction factors and form loss coefficients, different correlations have been used in the different sections of the facility. For the localized pressure drops, formulas have been taken from Ref. (Idelchik, 2003), while for the FPBS the Cheng and Todreas correlation for wire-wrapped tube bundles (Chen et al., 2013; Cheng and Todreas, 1986) has been used. RELAP5 allows the friction factor to be inversely proportional to Re in the laminar region, while a relation $\sim Re^{-C}$ can be selected in the turbulent region. In the transition region, identified by RELAP5 in the Re range between 2200 and 3000, the friction factor is the result of a linear interpolation between the two regions (Information System Laboratories, 2003). Therefore, the actual correlation has been approximated by the following equations in the Re range of interest, with the calibration coefficients reported in Table 5, and the graphical comparison is shown in Fig. 8.

$$\begin{cases} f_L = \dfrac{64}{\Phi_S \bullet Re} if Re < 2200 \\ f_{L,T} = \left(3.75 - \dfrac{8250}{Re}\right)\left(f_{T,3000} - f_{L,2200}\right) + f_{L,2200} if 2200 < Re < 3000 \\ f_T = A + B \bullet Re^{-C} if Re > 3000 \end{cases} \tag{3}$$

Further modeling issues arose from the analysis of the experimental data. The first consideration concerns the natural circulation regimes, i.e., the Steady State 2. The temperatures of the hot and cold legs, assumed equal to the TCs acquisitions at the FPBS and HX outlet, are 362.5 °C and 199.5 °C, respectively. The corresponding densities can be evaluated through the formulas reported in the benchmark specifications (Di Piazza et al., 2022), that coincide with the reference ones suggested by NEA in the 2015 HLMs Handbook (OECD/NEA, 2015). The resulting pressure head for the natural circulation can be calculated as follows:

$$\Delta p_{head} = \Delta\rho \bullet g \bullet H = (\rho_{@199.5^\circ C} - \rho_{@362.5^\circ C}) \bullet g \bullet H = 9.7 kPa \tag{4}$$

where $\Delta\rho$ is the density difference between the cold and hot leg, g is the gravitational constant, and H is the height difference between the FPBS

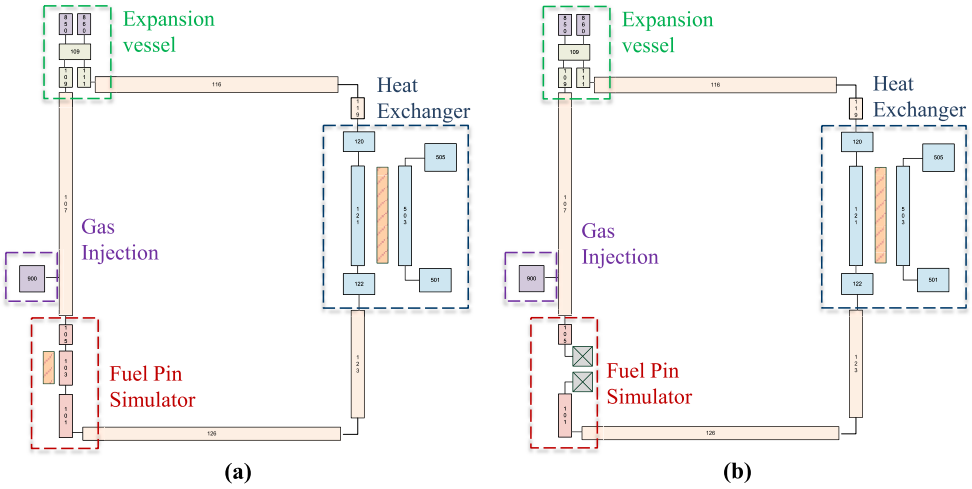

Fig. 7. Nodalization of the NACIE-UP loop: closed loop (on the left) and open loop (on the right).

Table 5
Coefficients for the calibration of the FPBS pressure drops in the RELAP5 model.

Constant	Φ_S	A	B	C
Value	0.45	0.021	31.66	0.856

and HX thermal barycenters.

The experimental mass flow in the final steady state (1.31 kg/s) corresponds to Re ~ 3600, from which a friction factor in the FPBS equal to 0.05 can be retrieved from Fig. 8. The pressure drops in the FPBS can be calculated as follows:

$$\Delta p_{FPBS} = \left(f \bullet \frac{L}{D_H}\right) \bullet \left(\frac{1}{2} \bullet \rho \bullet u^2\right) = 3.5kPa \quad (5)$$

In the previous, density and velocity refer to the inlet section of the FPBS. The pressure drops in the rest of the facility have been calculated analytically and numerically, i.e., from the RELAP5 simulation results. The comparison showed a good agreement between the two approaches, both resulting in very low values. This was expected since the velocities are very low in all the sections of the LBE primary loop, including the HX where the flow area is seven times larger than in the other sections of the loop, except for the FPBS. Details of the pressure drops distribution is reported in Table 6.

In conclusion, the only significant contribution to the total loop pressure drops is the one in the FPBS. The discrepancy between the values obtained with Eq. (4) and (5), i.e., between natural circulation driving force and circuit hydraulic resistance, could be attributed to an eventual additional pressure drop not considered in the models. A possible explanation of this pressure drop could be attributed to geometrical discontinuities created by – for instance – a deposit of oxides in the coldest part of the loop, i.e., the bottom of the downcomer, where the solubility of oxygen is the lowest. Such an eventual deposit may have reduced the flow area, locally increasing the pressure drops (Gladinez et al., 2020). Indeed, the experimental campaigns referred to the present benchmark were run without an online oxygen control system. To calibrate the numerical model, a concentrated pressure drop has been inserted at the bottom of the downcomer in the form of a constant K-coefficient.

With the model calibrated for the natural circulation regime, a simulation of only the first steady state has evidenced an under-prediction of the mass flow rate in forced circulation. This deviation is mainly due to a numerical underestimation of the void fraction profile

Table 6
Pressure drops along the loop in the Steady State 2.

Location	Pressure drop [kPa]
FPBS inlet elbow	0.11
FPBS pins	3.47
FPBS outlet grid	0.91
Riser	0.04
Expansion vessel (from inlet to outlet)	0.03
Upper horizontal leg	0.04
Upper bend	<0.01
HX	0.02
Downcomer	0.02
Lower bend	<0.01
Lower horizontal leg (including TFM)	0.10

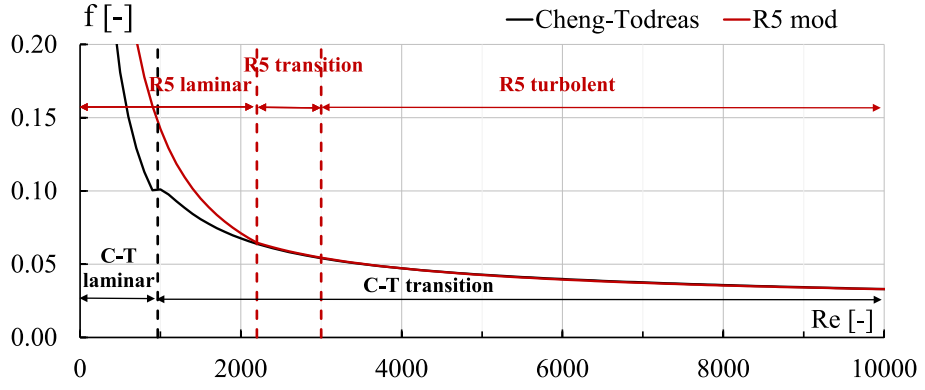

Fig. 8. Cheng and Todreas vs RELAP5 correlations for wire wrapped tube bundles.

within the riser. It is worth noticing that the gas lift has been simulated with a constant argon mass flow rate through a time dependent junction, with the gas TH conditions imposed by the time dependent volume represented by the purple box in Fig. 8. The coexistence of argon and LBE in the riser volume is allowed thanks to the modifications made to the code. However, it is important to note that, even in the modified version of RELAP5/Mod3.3, the drift-flux models adopted in the case of HLM/noncondensables are the same developed for the water/noncondensable case. During ADP10 and ADP06 tests, at Beginning of Transient, when forced circulation is promoted by the gas injection, the flow in the riser section is characterized by the following features: upflow and high mass flux (> 100 kg/m2s). In these conditions, the EPRI model is adopted by the code (Chexal et al., 1986). In particular, the computed average void fraction is half of the experimental one. Thus, the model proved to not be suitable for HLMs. For now, to compensate for this code limitation, the gas mass flow rate injected in the riser was doubled, matching in this way the void fraction profile calculated starting from the experimental data. Nevertheless, in the future developments of the activity, the authors are planning to implement more appropriate drift flux models for the HLM/noncondensable case.

4.3. CFD-RELAP5 coupled model

For the coupled simulation, the RELAP5 model has been modified removing the active part of the FPBS and inserting time dependent volumes (TMDPVOL) and time dependent junctions (TMDPJUN), where the BCs from the CFD calculation are imposed. The adopted approach is therefore the so-called "decomposition domain approach". A preliminary RELAP5 steady state calculation with the "open loop" model (see Fig. 7b) has been performed to prepare a restart file to be used for the coupled simulation. The BCs adopted for the "open loop" are the steady state values obtained with the entire loop.

During the coupled run the two-way exchange of information regards (see Fig. 9 for a graphical representation):

- the outlet mass flow rate (from Ansys CFX to RELAP5).
- the outlet temperature (from Ansys CFX to RELAP5).
- the total pressure drop along the active length of the FPBS (from Ansys CFX to RELAP5).
- the inlet mass flow rate (from RELAP5 to Ansys CFX).
- the inlet temperature in the FPBS (from RELAP5 to Ansys CFX).

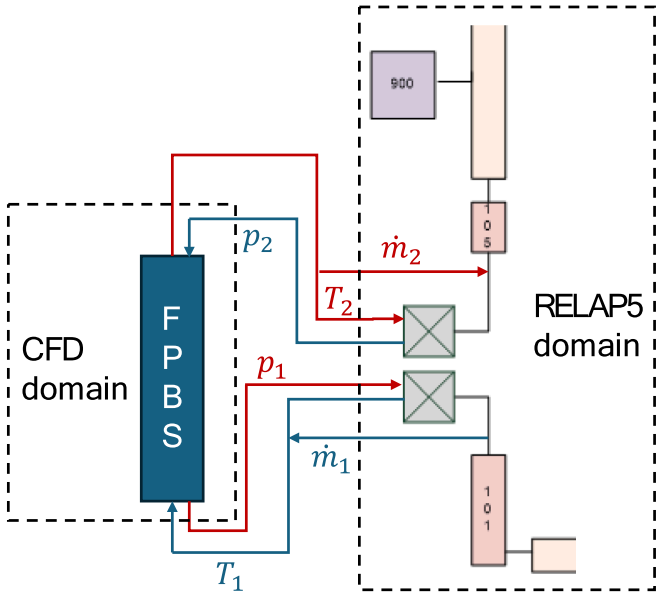

Fig. 9. Exchanged parameters in the coupled simulation.

The pressure drop is considered in the calculation of the absolute pressure at the outlet TMDPVOL in the RELAP5 domain (FPBS inlet), which is passed to RELAP5 and re-calculated at each timestep by means of the following equation:

$$p_1 = \Delta p_{fr,CFX} + \Delta p_{st} + p_2 \tag{6}$$

where:

- p_1 is the pressure at the FPBS inlet (see Fig. 9).
- $\Delta p_{fr,CFX}$ is the friction term (calculated by the CFD).
- Δp_{st} is the static term.
- p_2 is the absolute pressure at the FPBS outlet boundary computed by RELAP5 at the previous timestep (see Fig. 9). It is passed from RELAP5 to CFX only for calculating p_1 but it is not used as a boundary condition.

This method allows to set the relative pressure to zero at the outlet of the CFD model, with an impact in reducing the momentum equation residuals. The CFD inlet mass flow rate corresponds to the RELAP5 calculated value at the outlet of the "open loop". A non-dimensional velocity map has been imposed at the CFD inlet, obtained by averaging the two fully developed flow maps of the initial and final steady state CFD simulations. A similar procedure has been adopted to impose an inlet temperature distribution. The latter choices have been considered the best available solution to reduce computational time while conserving the overall simulation performance.

5. Results

5.1. System-level analysis

The steady states have been achieved through a 5000 s of null transient simulation with the constant BCs discussed in Sect. 2.2. Coupled simulations have been carried out with a constant time step both for the CFD and the RELAP5 codes, keeping the latter at 1/10 of the Ansys CFX time step, to improve the stability of the results. A preliminary sensitivity analysis has been performed varying the time step from 10^{-3} s to $2\bullet10^{-2}$ s, showing negligible differences. For the coupled simulations, a further null transient simulation of 10 s is performed to achieve a new steady state condition after the variable exchange between the codes. Only at this moment, the gas injection is stopped, and the transient is triggered.

Since in the considered experiments two different steady states are achieved, the comparison between the RELAP5, coupled tool, and experimental results for both the steady states for all the experiments are summarized in Table 7 and Table 8. The initial condition is named BOT (Beginning Of Transient) and the final condition is EOT (End Of Transient). The results of ADP10 and ADP06 tests do not significantly differ in terms of loop parameters since the FPBS power is the same, and the only difference is its distribution among the pins. By comparing the simulation results (both RELAP5 stand-alone and coupled) and the experimental data, the maximum discrepancy is related to the mass flow rate at BOT of the ADP06 test (~5%), comparable with the measurement uncertainty of the TFM. Instead, the maximum discrepancy for the temperatures can be found at the FPBS outlet at the EOT of the ADP10 test (about 12 °C). Since the predicted inlet temperature and mass flow rate are close to the experimental ones and the FPBS heat losses are negligible, the source of the deviation could be the value of the LBE specific heat capacity, with an unproper correlation implemented in the RELAP5/Mod3.3 code. This aspect is still under investigation.

As expected, the coupled simulation results well agree with the RELAP5 stand-alone ones, independently from the test. Moreover, the results between the two coupled calculations are almost the same since the boundary and initial conditions for the two tests are the same, except for the power distribution among the pins in the FPBS. The only

Table 7
Experimental vs RELAP vs coupled results (ADP10 test).

	Parameter	Unit	Exp	RELAP5	Error	Coupled	Error
BOT	LBE $\dot{m}$	kg/s	2.56	2.52	−1.6 %	2.60	1.6 %
	T in FPBS	°C	225.56	223.16	−2.40 °C	223.25	−2.31 °C
	T out FPBS	°C	305.24	299.03	−6.21 °C	299.74	−5.50 °C
	T in HX	°C	301.58	296.93	−4.65 °C	295.05	−6.53 °C
	T out HX	°C	220.53	218.62	−1.91 °C	218.79	−1.74 °C
EOT*	LBE $\dot{m}$	kg/s	1.31	1.34	2.3 %	–	–
	T in FPBS	°C	207.45	207.22	−0.23 °C	–	–
	T out FPBS	°C	362.44	350.45	−11.99 °C	–	–
	T in HX	°C	353.28	345.94	−7.34 °C	–	–
	T out HX	°C	199.36	200.02	0.66 °C	–	–

* Results of the coupled calculation at EOT are not available since it ends at 1500 s

Table 8
Experimental vs RELAP vs coupled results (ADP06 test).

	Parameter	Unit	Exp	RELAP5	Error	Coupled	Error
BOT	LBE $\dot{m}$	kg/s	2.66	2.52	−5.3 %	2.60	−2.3 %
	T in FPBS	°C	227.67	223.40	−4.27 °C	223.25	−4.42 °C
	T out FPBS	°C	304.35	299.27	−5.08 °C	300.32	−4.03 °C
	T in HX	°C	301.39	297.22	−4.17 °C	295.05	−6.34 °C
	T out HX	°C	222.74	218.80	−3.94 °C	218.79	−3.95 °C
EOT*	LBE $\dot{m}$	kg/s	1.33	1.34	−0.8 %	–	–
	T in FPBS	°C	207.67	207.33	−0.34 °C	–	–
	T out FPBS	°C	359.93	350.56	−9.37 °C	–	–
	T in HX	°C	351.20	346.18	−5.02 °C	–	–
	T out HX	°C	199.62	200.11	0.49 °C	–	–

* Results of the coupled calculation at EOT are not available since it ends at 1500 s

difference can be noticed on the FPBS (CFD domain) outlet temperature, while all the other quantities are calculated by RELAP5.

The instant when the gas injection is stopped is the Start of the Transient (SoT) and it is assumed to be at t = 0 s for both the RELAP5 and coupled simulations. The thermal power provided by the FPBS remains constant, as well as the water temperature and mass flow rate at the HX secondary side. As done for the steady states, also for the transient phase, the global comparison between experimental data and the RELAP5 and coupled results involves only the loop parameters since local temperatures in the FPBS cannot be well predicted by the STH code.

As shown in Fig. 10 and Fig. 11, the LBE mass flow rate rapidly drops to ~1 kg/s as soon as the gas injection is stopped, and after ~1500 s (that is the time considered for the coupled simulation) a new steady state establishes after the transition to the natural circulation regime. The delay in the experimental mass flow rate drop down can be attributed to the intrinsic delay in the measurement of the thermal flow meter and not to physical reasons. Indeed, the same delay is not present in the TCs acquisitions, as shown by the timing of the FPBS temperature excursions in Fig. 12 and Fig. 13 that is in good agreement between tests and simulation results. In fact, FPBS temperatures quickly respond to mass flow variation since the FPBS is characterized by an imposed heat flux, thus temperatures change accordingly to mass flow variations. In Fig. 14 and Fig. 15, a zoom at the beginning of the transient better shows the discrepancy of the mass flow variation with respect to the experimental value, while a good agreement is obtained for the temperatures. As for the steady state results, the curves of the coupled simulations almost overlap the RELAP5 stand-alone results since the transition is governed by phenomena that can be represented by a 1D model. The small discrepancies can be addressed to a more detailed modeling of the FPBS, and a different evaluation of the pressure drops in the component.

Fig. 12 and Fig. 13 show a good agreement between experimental and numerical values of the FPBS inlet and outlet temperatures, confirming the correct representation of the mass flow rate transition, while a certain delay can be observed in the HX inlet and outlet temperature (see Fig. 16 and Fig. 17), probably due to a not complete representation

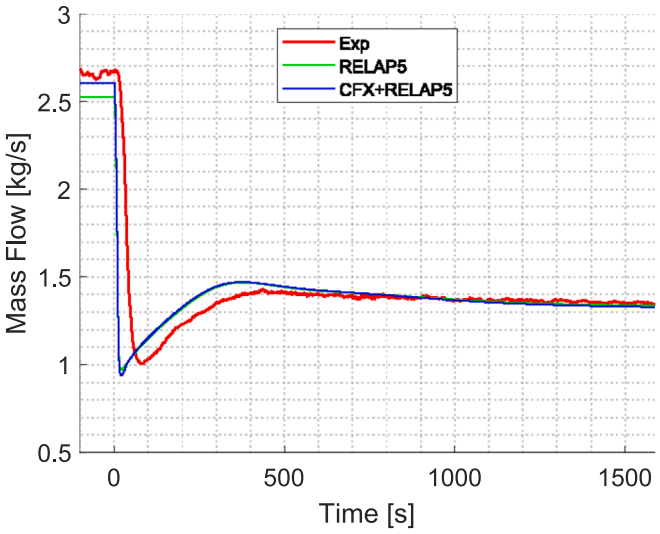

Fig. 10. Experimental vs RELAP5 vs coupling mass flow rate comparison (ADP06).

of the heat capacity in the system. In fact, part of the metallic structure of the shell is not simulated because of its minor impact on the phenomenology and its complex geometry, but its effect is visible in the medium term (500–1000 s). Again, the numerical trends predicted by RELAP5, and the coupled tool are very close to each other, meaning that a 1D representation of the entire system in these conditions is sufficient for a proper description of the loop TH phenomena.

In this situation, the main advantage of applying the coupled tool is the possibility to perform CFD level analysis on the FPBS providing appropriate BCs in terms of mass flow rate and inlet temperature from a system level calculation (RELAP5), keeping a reasonable computational time.

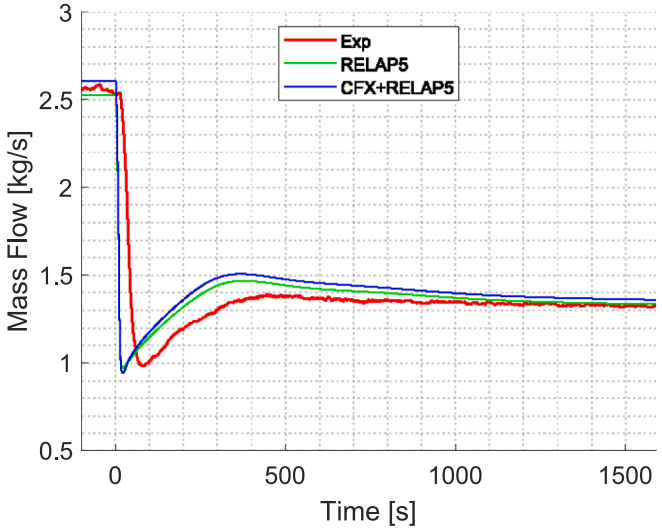

Fig. 11. Experimental vs RELAP5 vs coupling mass flow rate comparison (ADP10).

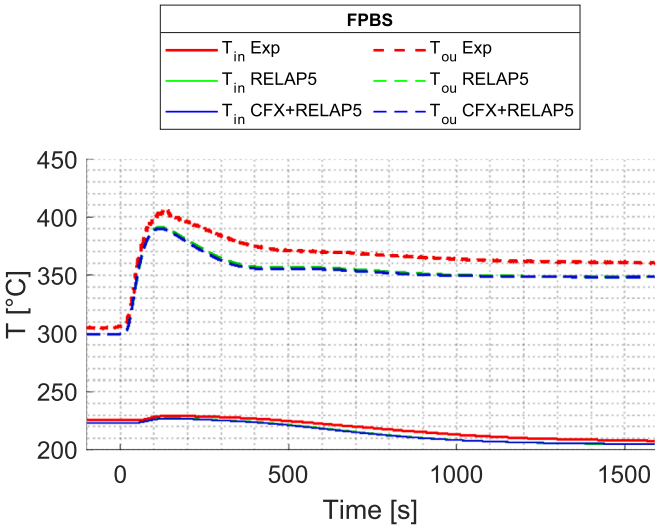

Fig. 13. Experimental vs RELAP5 vs coupling FPBS temperature comparison (ADP10).

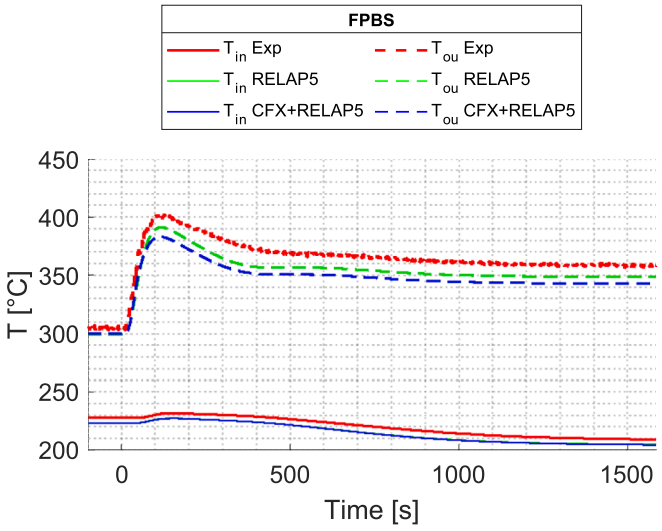

Fig. 12. Experimental vs RELAP5 vs coupling FPBS temperature comparison (ADP06).

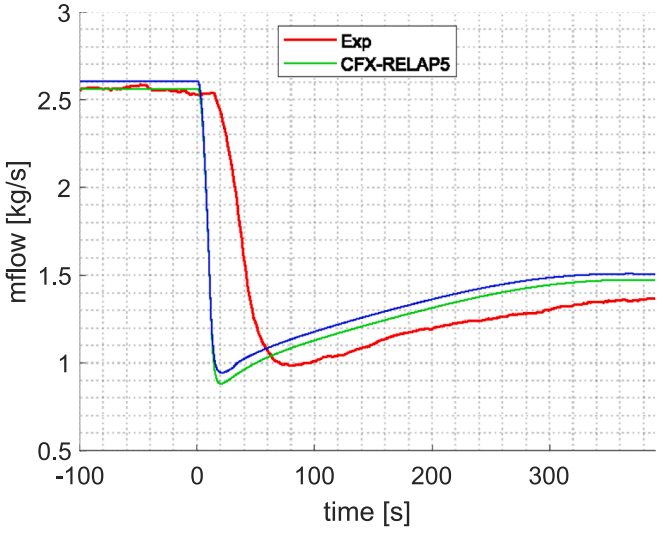

Fig. 14. Experimental vs RELAP5 vs coupling mass flow rate comparison at the beginning of the transient (ADP10).

5.2. FPBS detailed component analysis

CFD and experimental data have been compared focusing on the local temperatures in 67 TCs positions. The experimental BCs are described in section 2 and reported in (Di Piazza et al., 2022), together with the TCs locations.

For what concerns the steady state simulation corresponding to the BOT, the results are reported in Fig. 18 and Fig. 19 for ADP06 and ADP10, respectively. The plots report experimental and numerical data as a function of the thermocouple number. The overall x-axis is divided into three sections referred to bulk, wall and Pin 3 TCs. Data referred to bulk and wall TCs are at their time subdivided considering the three axial instrumented planes, reminding that the position of their TCs within the transversal section is the same.

The Ansys CFX model results show good qualitative agreement with the experimental data with an average error lower than 5 °C in both cases (Table 9). The ADP10 case exhibits the most uniform characteristics, with lower gradients, and can be represented with very minimal discrepancies across the entire domain. The ADP06 introduces non uniformity with a non-heated region in the last rank of the bundle. Even in this case, the overall trend of the CFD temperatures matches the experimental one, however, it could be noticed that the internal region (the heated one) temperatures are overestimated, while the external ones underestimated. The reason could be an underestimation of the radial velocities due to turbulence generated by the wires. Fig. 20 and Fig. 21 show the temperature difference between CFX and experiments at the Plane 3 TCs locations: both cases exhibit the described behavior, with higher error values in the ADP06 case.

Errors on the first measurement plane could be caused by the simplified approach of considering only the active length and thus not simulating in the CFD domain the hydraulic and thermal flow development before the active length. However, the error magnitude is in the same range as the one in the second plane demonstrating the effectiveness of a properly imposed velocity map. In general, the third plane presents the higher differences with the experimental results. The pin 3 thermocouples show in both tests a good qualitative agreement along the entire heated length.

Fig. 22 and Fig. 23 show the comparison between the experimental results and the numerical trends, obtained by the coupled tool, of local temperatures inside the FPBS, in particular TC 12 (bulk) and TC 49

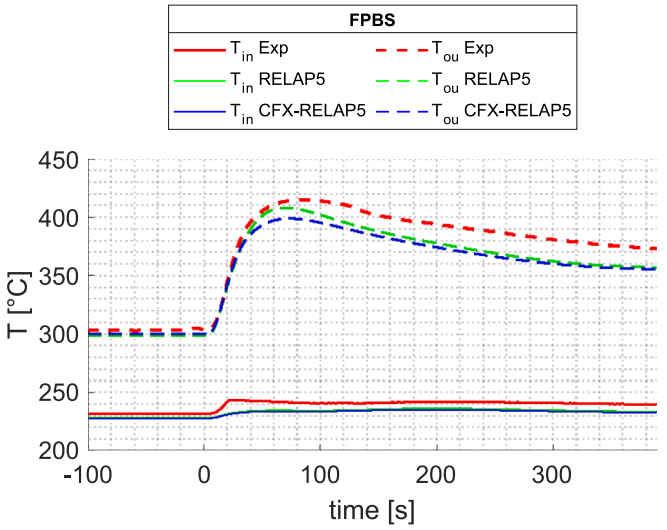

Fig. 15. Experimental vs RELAP5 vs coupling FPBS temperature comparison at the beginning of the transient (ADP10).

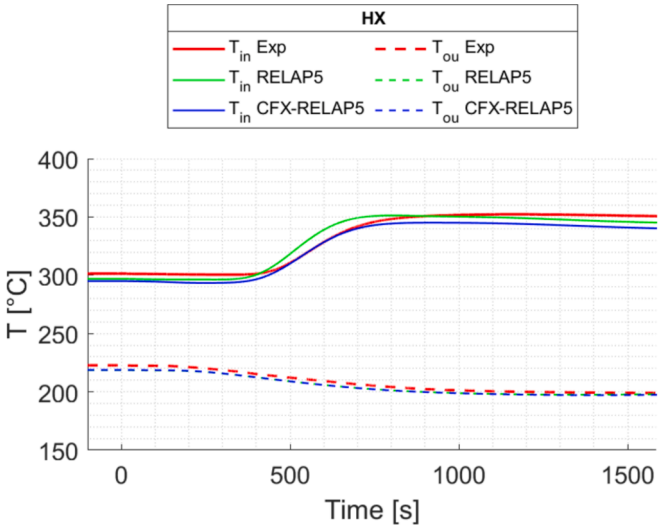

Fig. 16. Experimental vs RELAP5 vs coupling HX temperature comparison (ADP06).

(wall), reported as example. The CFD calculation demonstrates to reproduce with similar behavior the experimental results. The error is lower at the initial steady state and going toward the end of the transient, thus approaching steady state conditions. The differences in the transient region could be explained by considering the discrepancy between experimental and numerical LBE mass flow rate, already discussed in the previous section.

6. Conclusions

The paper presents a numerical application of an in-house developed CFD-STH coupled tool applied to the LBE-cooled loop facility NACIE-UP. The experimental tests considered (ADP10 and ADP06) consist in a transition from forced to natural circulation regimes in a HLM loop.

The key features of the coupled tool have been described together with the stand-alone models of the RELAP5 and Ansys CFX codes. Preliminary calibration is required for the two stand-alone models to better match the experimental results, thus giving more reliable results in the coupled simulations. The RELAP5 results showed a good agreement for the mass flow rate, and a maximum error of 12 °C in the temperature in

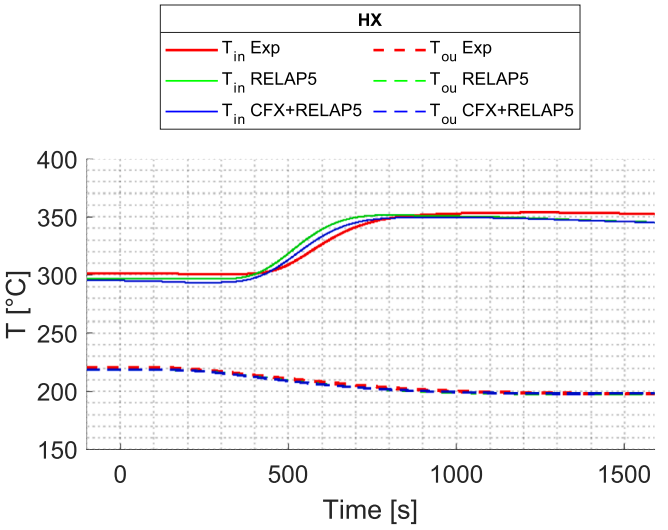

Fig. 17. Experimental vs RELAP5 vs coupling HX temperature comparison (ADP10).

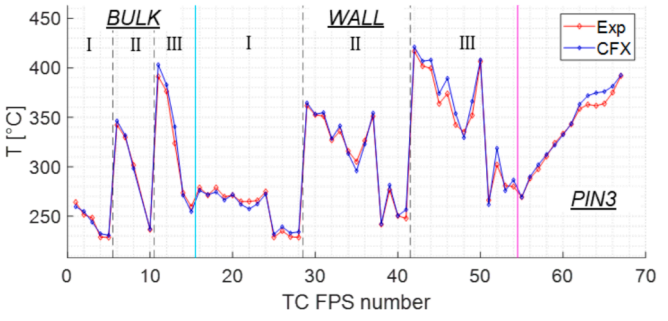

Fig. 18. TCs temperature comparison for the BOT steady state, ADP06.

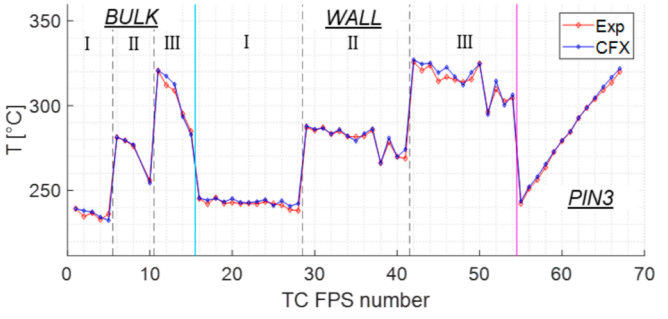

Fig. 19. TCs temperature comparison for the BOT steady state, ADP10.

Table 9
Mean and maximum temperature difference between CFD and experiment at BOT.

$\Delta T_{ExpvsCFX}$ [°C]	ADP10		ADP06	
	mean	max	*mean*	max
Error Plane 1	1.66	4.27	3.48	7.61
Error Plane 2	1.04	5.33	4.06	11.92
Error Plane 3	2.69	5.62	7.72	16.75
Error Tot	1.68	5.62	4.98	16.75

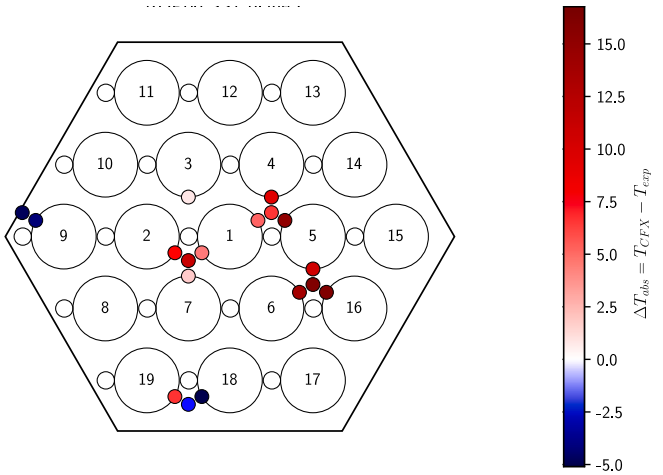

Fig. 20. Ansys CFX BOT steady state, temperature comparison on Plane 3 (ADP06).

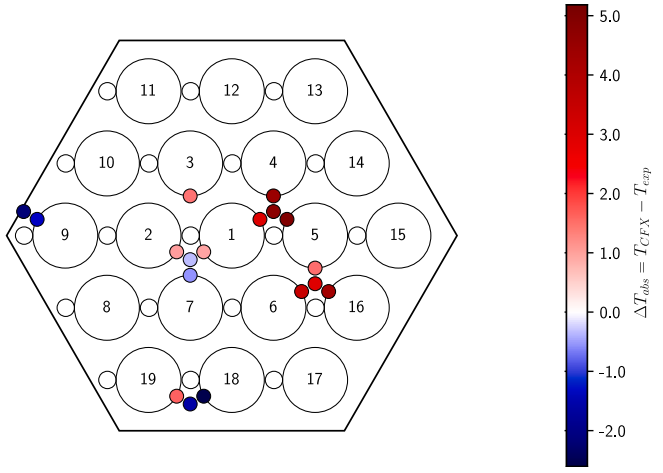

Fig. 21. Ansys CFX BOT steady state, temperature comparison on Plane 3 (ADP10).

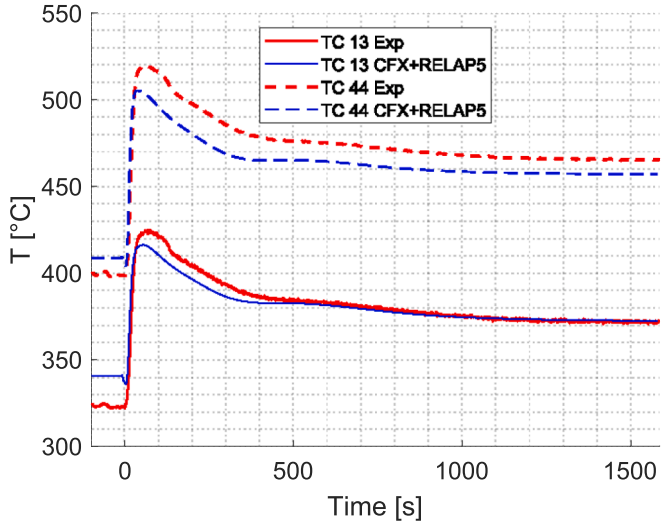

Fig. 22. Experiment vs coupling TC13 and TC44 temperature comparison (ADP06).

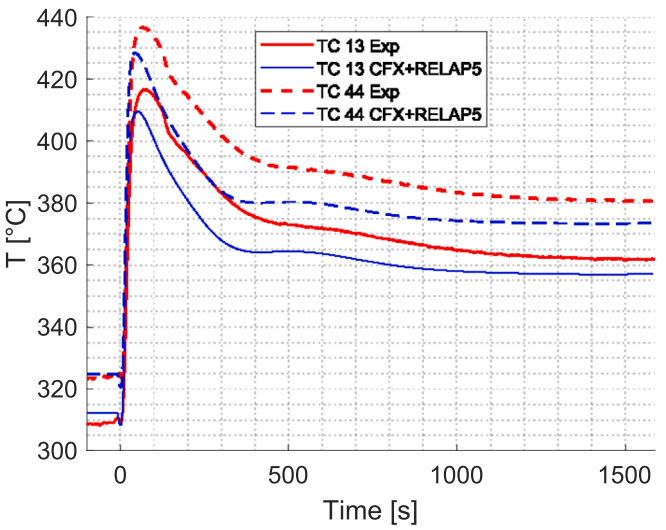

Fig. 23. Experiment vs coupling TC13 and TC44 temperature comparison (ADP10).

the steady states analyzed. The CFD calculation of the initial steady state showed an average error in the local FPBS temperatures lower than 5 °C for both cases. The qualitative representation of the thermal field is in good agreement with the experimental results. The non-uniform power generation in the ADP06 test could have caused an enhancement of the radial component of the velocity with respect to the ADP10 case, which has not been well predicted by the code.

The coupled model has been obtained by removing the active part of the FPBS from the RELAP5 domain, adopting the so-called "decomposition domain approach". The adopted time scheme is semi-implicit, resulting in a more stable solutions execution compared to the explicit one. The obtained mass flow rate and temperatures are close to the RELAP5 stand-alone results, with small discrepancies in the investigated time window (1500 s transient). The coupling approach has given similar results compared to the RELAP5 stand-alone simulation. However, the scope of developing the coupling tool is not obtain better results than STH and CFD codes in their respective domains (i.e., system-level and component-level analyses). Instead, its main advantage is the possibility to obtain with a single calculation the detailed local description of the FPBS active region (CFD domain), being the main TH phenomena governing the considered transients analyzable with STH codes. Errors in the local FPBS temperatures during the coupled transient simulation are linked to the inaccuracies in reproducing system level quantities such as the mass flow rate.

In this work, it has been shown that the coupled tool gives results consistent with the RELAP5 one in a case where 1D effects are dominant. Future applications of the tool will focus on cases where the CFD feedback is expected to significantly improve the simulation results, such as pool-type systems where mixing/thermal stratification phenomena play a key role in a transient evolution.

CRediT authorship contribution statement

T. Del Moro: Writing – original draft, Software, Methodology, Investigation, Conceptualization. **P. Cioli Puviani:** Writing – review & editing, Software, Methodology, Investigation, Conceptualization. **B. Gonfiotti:** Writing – review & editing, Software. **I. Di Piazza:** Writing – review & editing, Data curation. **D. Martelli:** Writing – review & editing. **C. Ciurluini:** Writing – review & editing. **F. Giannetti:** Writing – review & editing, Supervision. **R. Zanino:** Writing – review & editing. **M. Tarantino:** Writing – review & editing, Supervision.

Declaration of competing interest

The authors declare the following financial interests/personal relationships which may be considered as potential competing interests: Tommaso Del Moro reports writing assistance was provided by ENEA Brasimone Research Centre. Tommaso Del Moro reports a relationship with ENEA Brasimone Research Centre that includes: funding grants. If there are other authors, they declare that they have no known competing financial interests or personal relationships that could have appeared to influence the work reported in this paper..

Acknowledgements

The data and information presented in the paper are part of an ongoing IAEA coordinated research project on “Transition from Forced to Natural Circulation Experiment with Heavy Liquid Metal Loop – CRP-I31038”.

Data availability

The data that has been used is confidential.

References

Alemberti, A., Frignani, M., Villabruna, G., P. Agostini, G. Grasso, M. Tarantino, I. Turcu, M. Constantin, D. Diaconu, F. Di Gabriele, N. Witzanyova, M. Krykova, ALFRED and the lead technology research infrastructure, Proceedings of European Research Reactor Conference (RRFM), Bucharest, Romania, April 19-23, 2015.

Angelucci, M., Di Piazza, I., Tarantino, M., Marinari, R., Polazzi, G., Sermenghi, V., Experimental tests with non-uniformly heated 19-pins fuel bundle cooled by HLM, ICONE26-81216, Proc. ICONE26, July 22–26, 2018, London. https://doi.org/10.1115/ICONE26-81216.

ANSYS CFX-Solver Theory Guide, November 2011.

ANSYS FLUENT 12.0 Theory Guide, January 2009.

Argonne National Laboratory. SAM: A Modern System Analysis Tool for Advanced Nuclear Reactors, https://www.anl.gov/nse/system-analysis-module.

Aumiller, D.L., Tomlinson, E.T., Bauer, R.C., 2001. A coupled RELAP5-3D/CFD methodology with a proof-of-principle calculation. Nucl. Eng. Des. 205, 83–90. https://doi.org/10.1016/S0029-5493(00)00370-8.

Bertolotto, D., Manera, A., Frey, S., Prasser, H.-M., Chawla, R., 2009. Single-phase mixing studies by means of a directly coupled CFD/system-code tool. Ann. Nucl. Energy 36 (3), 310–316. https://doi.org/10.1016/j.anucene.2008.11.027.

CEA, CATHARE 2 v25_3mod9.1 code: General description, NT/2019-65638/A, November 2019.

Chen, S.K., Petroski, R., Todreas, N.E., 2013. Numerical implementation of the Cheng and Todreas correlation for wire wrapped bundle friction factors-desirable improvements in the transition flow region. Nucl. Eng. Des. 263, 406–410. https://doi.org/10.1016/j.nucengdes.2013.06.012.

Cheng, S.K., Todreas, N.E., 1986. Hydrodynamic models and correlations for bare and wire-wrapped hexagonal rod bundles — Bundle friction factors, subchannel friction factors and mixing parameters. Nucl. Eng. Des. 92 (2), 227–251. https://doi.org/10.1016/0029-5493(86)90249-9.

Chexal, B., Lellouche, G., 1986. A Full-Range Drift-Flux Correlation for Vertical Flows (Revision 1), EPRI NP-3989-SR, Electric Power Research Institute, September 1986. Available online at: https://www.epri.com/research/products/NP-3989-SR. Last visited: 19/09/2024.

Cioli Puviani, P., Venturini, A., Di Piazza, I., Sermenghi, V., Del Moro, T., Papa, F., Martelli, D., Zanino, R., Tarantino, M., 2024. Development of a thermal mass flow meter for heavy liquid metal applications. Nucl. Eng. Des. 427, 113427. https://doi.org/10.1016/j.nucengdes.2024.113427.

Cioli Puviani, P., Del Moro, T., Gonfiotti, B., Martelli, D., Giannetti, F., Zanino, R., Tarantino, M., 2025. A novel Ansys CFX – RELAP5 coupling tool for the transient thermal-hydraulic analysis of liquid metal systems. Prog. Nucl. Energy.

Cioli Puviani, P., Di Piazza, I., Marinari, R., Zanino, R., Tarantino, M., 2022. Multiscale Thermal-Hydraulic Analysis of the ATHENA Core Simulator, ICONE29-93457, V008T08A064, 23 November 2022. https://doi.org/10.1115/ICONE29-93457.

Cioli Puviani, P., Zanino, R., Del Moro, T., Giannetti, F., Gonfiotti, B., Di Piazza, I., Martelli, D., Tarantino, M., CFD - STH Code Coupling for the Thermal Hydraulic Analysis of NACIE-UP Experimental Facility, pp. 3638–3651, 20th International Topical Meeting on Nuclear Reactor Thermal Hydraulics (NURETH-20), Washington, D.C., USA, 10.13182/NURETH20-40088.

Ciurluini, C., Marra, M., Narcisi, V., Caruso, G., Giannetti, F., 2024. Investigation of the fast flux test facility transient behavior during a loss of flow without scram test. Nucl. Eng. Des. 428, 113534. https://doi.org/10.1016/j.nucengdes.2024.113534.

Di Piazza, I., Angelucci, M., Marinari, R., Tarantino, M., Martelli, D., 2019. Thermo-fluid dynamic transients in the NACIE-UP facility. Nucl. Eng. Des. 352, 110182. https://doi.org/10.1016/j.nucengdes.2019.110182.

Di Piazza, I., Hassan, H., Lorusso, P., Martelli, D., 2022. Benchmark Specifications For Nacie-Up Facility: Non-Uniform Power Distribution Tests, ENEA Report ID: NA-I-R-542, CR Brasimone, 22 July 2022.

Dragunov, Y.G., Lemekhov, V.V., Smirnov, V.S., Chernetsov, N.G., 2012. Technical solutions and development stages for the BREST-OD-300 reactor unit. Atomic Energy 113 (1). https://doi.org/10.1007/s10512-012-9597-3.

Forgione, N., Angelucci, M., Ulissi, C., Martelli, D., Barone, G., Ciolini, R., Tarantino, M., 2019. Application of RELAP5/Mod3.3 – fluent coupling codes to CIRCE-HERO. J. Phys. Conf. Ser. 1224. https://doi.org/10.1088/1742-6596/1224/1/012032.

Forgione, N., Martelli, D., Barone, G., Giannetti, F., Lorusso, P., Hollands, T., Papukchiev, A., Polidori, M., Cervone, A., Di Piazza, I., 2019. Post-test simulations for the NACIE-UP benchmark by STH codes. Nucl. Eng. Des. 353, 110279. https://doi.org/10.1016/j.nucengdes.2019.110279.

Frignani, M., Alemberti, A., Villabruna, G., Adinolfi, R., Tarantino, M., Grasso, G., Pizzuto, A., Turcu, I., Valeca, S., 2017. ALFRED: A Strategic Vision for LFR Deployment. Transactions of the American Nuclear Society, Washington, D.C.

Frignani, M., Alemberti, A., Tarantino, M., 2019. ALFRED: A revised concept to improve pool related thermal-hydraulics. *Nucl. Eng. Des.* 335 (15). https://doi.org/10.1016/j.nucengdes.2019.110359.

Generation IV International Forum (GIF), https://www.gen-4.org/gif/.

Gladinez, K., Rosseel, K., Lim, J., Shin, Y.H., Heynderickx, G., Aerts, A., 2020. Determination of the lead oxide fouling mechanisms in lead bismuth eutectic coolant. Nucl. Eng. Des. 357 (110382). https://doi.org/10.1016/j.nucengdes.2019.110382.

Grishchenko, D., Jeltsov, M., Kööp, K., Karbojian, A., Villanueva, W., Kudinov, P., 2015. The TALL-3D facility design and commissioning test for validation of coupled STH and CFD codes. Nucl. Eng. Des. 290, 144–153. https://doi.org/10.1016/j.nucengdes.2014.11.045.

GRS, ATHLET 3.3 User's Manual, Report GRS-P-1/Vol.1 Rev.9, November 2021.

Grunloh, T.P., Manera, A., 2016. A novel domain overlapping strategy for the multiscale coupling of CFD with 1D system codes with applications to transient flows. Ann. Nucl. Energy 90, 422–432. https://doi.org/10.1016/j.anucene.2015.12.027.

Grunloh, T.P., Manera, A., 2017. A novel multi-scale domain overlapping CFD/STH coupling methodology for multi-dimensional flows relevant to nuclear applications. Nucl. Eng. Des. 318, 85–108. https://doi.org/10.1016/j.nucengdes.2017.03.027.

https://www.newcleo.com/.

Huxford, A., Coppo Leite, V., Merzari, E., Zou, L., Petrov, V., Manera, A., 2023. A hybrid domain overlapping method for coupling System Thermal Hydraulics and CFD codes. Ann. Nucl. Energy 189 (109842). https://doi.org/10.1016/j.anucene.2023.109842.

Huxford, A., Zou, L., Hu, R., Petrov, V., Manera, A., 2024. Validation of a hybrid domain overlapping coupling between SAM and CFD against the TALL-3D transients. Nucl. Technol. 1–8. https://doi.org/10.1080/00295450.2024.2352665.

Idelchik, I.E., 2003. Handbook of Hydraulic Resistance, 3rd ed. Jaico Publishing House.

Information System Laboratories, RELAP5/Mod3.3 code manual volume I: code structure, system models, and solution methods, July 2003.

Li, W., Wu, X., Zhang, D., Su, G., Tian, W., Qiu, S., 2014. Preliminary study of coupling CFD code FLUENT and system code RELAP5. Ann. Nucl. Energy 73, 96–107. https://doi.org/10.1016/j.anucene.2014.06.042.

Lorusso, P., Bassini, S., Del Nevo, A., Di Piazza, I., Giannetti, F., Tarantino, M., Utili, M., 2018. GEN-IV LFR development: Status & perspectives. Progr. Nucl. Energy 105, 318–331. https://doi.org/10.1016/j.pnucene.2018.02.005.

Lorusso, P., Del Nevo, A., Narcisi, V., Giannetti, F., Caruso, G., Zwijsen, K., Breijder, P.A., Hamidouche, T., Castelliti, D., Rozzia, D., Tarantino, M., 2021. Total loss of flow benchmark in CIRCE-HERO integral test facility. Nucl. Eng. Des. 376, 1110864. https://doi.org/10.1016/j.nucengdes.2021.111086.

Marinari, R., Di Piazza, I., Tarantino, M., Angelucci, M., Martelli, D., 2019. Experimental tests and post-test analysis of non-uniformly heated 19-pins fuel bundle cooled by Heavy Liquid Metal. Nucl. Eng. Des. 343, 166–177. https://doi.org/10.1016/j.nucengdes.2018.12.024.

Martelli, D., Forgione, N., Barone, G., Di Piazza, I., 2017a. Coupled simulations of the NACIE facility using RELAP5 and ANSYS FLUENT codes. Ann. Nucl. Energy 101, 408–418. https://doi.org/10.1016/j.anucene.2016.11.041.

Martelli, E., Giannetti, F., Ciurluini, C., Caruso, G., 2019. Thermal hydraulic modeling and analyses of the water cooled EU DEMO using RELAP5 system code. Fusion Eng. Des. 146 (Part A), 1121–1125. https://doi.org/10.1016/j.fusengdes.2019.02.021.

Martelli, D., Ranieri Marinari, G., Barone, I.D., Piazza, M.T., 2017b. CFD thermo-hydraulic analysis of the CIRCE fuel bundle. Ann. Nucl. Energy 103, 294–305. https://doi.org/10.1016/j.anucene.2017.01.031.

Moreau, V., Profir, M., Alemberti, A., Frignani, M., Merli, F., Belka, M., Frybort, O., Melichar, T., Tarantino, M., Franke, S., Eckert, S., Class, A., Yanez, J., Grishchenko, D., Jeltsov, M., Kudinov, P., Roelofs, F., Zwijsen, K., Visser, D.C., Badillo, A., Niceno, B., Martelli, D., 2019. Pool CFD modelling: Lessons from the sesame project. Nucl. Eng. Des. 355, 110343. https://doi.org/10.1016/j.nucengdes.2019.110343.

Handbook on lead-bismuth eutectic alloy and lead properties, material compatibility, thermal-hydraulics and technologies. OECD/NEA, 2015. https://inis.iaea.org/collection/NCLCollectionStore/_Public/46/133/46133907.pdf.

Oriolo, F., Ambrosini, W., Forgione, N., Napoli, A., Tarantino, M., 2000. Modifiche del Codice RELAP5 versione MOD3.2 per la Simulazione di Sistemi Refrigerati con leghe di Pb o Pb-Bi. University of Pisa.

Pucciarelli, A., Toti, A., Castelliti, D., Belloni, F., Van Tichelen, K., Moscardini, M., Galleni, F., Forgione, N., 2020. Coupled system thermal Hydraulics/CFD models: General guidelines and applications to heavy liquid metals. Ann. Nucl. Energy 153, 107990. https://doi.org/10.1016/j.anucene.2020.107990.

Siemens 2021 STAR-CCM+ User Manual [Online]. Available: https://docs.sw.siemens.com/documentation/external/PL20200617112215329/en-US/userManual/userGuide/ html/index.html#page/connect%2Fsplash.html.

Toti, A., Vierendeels, J., Belloni, F., 2016. Development and Preliminary Validation of a STH-CFD Coupling Method for MYRRHA Reactor Simulations, *Proceedings of the 24th International Conference on Nuclear Engineering (ICONE24)*, Paper No. ICONE24-60438. DOI: 10.1115/ICONE24-60438.

USNRC, TRACE V5.0 Developmental Assessment Manual, ADAMS ML120060208, ML120060187, ML120060191, ML120060172, 2008.

Westinghouse, Lead-cooled Fast Reactor (LFR): The Next Generation of Nuclear Technology, https://www.westinghousenuclear.com/energy-systems/lead-cooled-fast-reactor/.